J. Appl. Comput. Mech., 8(4) (2022) 1186-1195
DOI: 10.22055/JACM.2020.33703.2272

ISSN: 2383-4536
jacm.scu.ac.ir

Shahid Chamran University of Ahvaz

Journal of Applied and Computational Mechanics

Research Paper

Characterization of the Nonlinear Biaxial Mechanical Behavior of Human Ureter using Constitutive Modeling and Artificial Neural Networks

Behzad Seyfi, Aisa Rassoli, Milad Imeni Markhali, Nasser Fatouraee

Department of Biomedical Engineering, Amirkabir University of Technology (Tehran PolyTechnic), Tehran, Iran
Email Addresses: b.seyfi@aut.ac.ir/ aisa.rassoli@gmail.com/ milad_imeni@yahoo.com/ nasser@aut.ac.ir

Received May 22 2020; Revised July 29 2020; Accepted for publication August 03 2020.
Corresponding author: B. Seyfi (b.seyfi@aut.ac.ir)

Abstract. Characterization of the mechanical properties of soft biological tissues is a fundamental issue in a variety of medical applications. As such, constitutive modeling of biological tissues that serves to establish a relationship between the kinematic variables has been used to formulate the tissue's mechanical response under various loading conditions. However, the validation of the developed analytical and numerical models is accompanied by a length of computation time. Hence, the need for new advantageous methods like artificial intelligence (AI), aiming at minimizing the computation time for real-time applications such as in robotic-assisted surgery, sounds crucial. In this study, at first, the mechanical nonlinear characteristics of human ureter were obtained from planar biaxial test data, in which the examined specimens were simultaneously loaded along their circumferential and longitudinal directions. To do so, the biaxial stress-strain data was used to fit the well-known Fung and Holzapfel-Delfino hyperelastic functions using the genetic optimization algorithm. Next, the potential of Artificial Neural Networks (ANN), as an alternative method for prediction of the mechanical response of the tissue was evaluated such that, multilayer perceptron feedforward neural network with different architectures was designed and implemented and then, trained with the same experimental data. The results showed both approaches were practically able to predict the ureter nonlinearity and in particular, the ANN model can follow up the tissue nonlinearity during the entire loading phase in both low and high strain amplitudes (RMSE<0.02). Such results confirmed that neural networks can be a reliable alternative for modeling the nonlinear mechanical behavior of soft biological tissues.

Keywords: Soft tissue modeling, Ureter, Nonlinear mechanical properties, Biaxial test, Artificial Intelligent.

1. Introduction

The ureters are paired fibromuscular thin (3 to 4 mm) tubes with narrow lumina that act to transport urine from the renal pelvis to the bladder using peristaltic mechanism exerted by the muscular layers of the ureter wall Considering this conveying mechanism, the ureter as a neuromuscular structure has remarkable clinical importance [1, 2]. Several pathological conditions affect the normal functionality of the ureter. For instance, megaureter as one of the most important abnormalities of the upper urinary tract is classified by some urologists into refluxing, obstructive, non-refluxing, and non-obstructive cases [3, 4]. All of which are directly related to bilateral effects of the alteration in pathological conditions and mechanical properties of the ureteral wall, undergoing large deformations (nonlinearity), and ureteral peristalsis. Furthermore, like arterial walls, any distortion of the directional organization of collagen fibers (i.e. circumferential and longitudinal directions) may be important in triggering the onset of megaureters [5]. Given the mentioned problem, the mechanical characterization of the ureter tissue is of great benefit to diverse groups of researchers for medical diagnosis, medical imaging technology, robotic surgeries, tissue engineering or for finite element (FE) and fluid-solid interaction (FSI) analyses [6-8]. To mark these applications, studies show that during the past decade, robotics and surgical simulation have been increasingly used in numerous procedures in urology [1], in which biomechanical models are supposed to compensate for undesirable movements such as breathing and heart beating motion during the operation [9]. To carry out high-performance surgery, these models should encapsulate a priori knowledge about the mechanical behavior of soft tissue for subsequent predictions.

Typically, the mechanical characterizations involve a level of complexity in soft tissue modeling originating from the specific architecture of each category of soft tissues which in turn is specialized for their pertinent functions. Thus, several investigations into the mechanical modeling of different types of soft biological tissues such as arterial wall, brain, liver, kidney, and cartilage have been done in the framework of constitutive modeling [10-14]. Despite these efforts and considering the correlation between the pathological and clinical interpretation of the ureteral elasticity, little classified information is available in the literature about the mechanical behavior of ureteral wall [2, 5, 15].

Published online: March 26 2021

Conventionally, there are three predominant approaches for the mechanical characterization of soft tissues: phenomenological, continuum-based, and structural. Each of these methods has its own benefits and drawbacks. The phenomenological approach uses experimentally gathered data derived from the mechanical response of a tissue (e.g. stress-strain curves) and afterward, fits them into mathematical expressions. The continuum method describes tissues as a divisible mixture and uses constitutive equations to refer to explicit terms for material properties of each contribution, namely the solid phase, the fluid phase, the cells, the extracellular matrix (ECM), and the interaction between the cells, the ECM and fibers. To control the complexity of this approach, structural models, involve the ultrastructure directly and follow the hypothesis that the overall mechanical behavior of the tissue stems from the sum of the micro-responses of its components [16]. Despite the accuracy of these methods for numerical realization using the finite element method, they would suffer from high computational costs when the tissue structure and/or mechanical behavior are spatially variable [8]. Practically, the validation of the developed models takes two steps: conducting experimental tests and solving the inverse problems for obtaining models' unknown parameters. Depending on different criteria such as study purpose and tissue structure, there are several ways for performing each step.

Even though, the aforementioned validation procedure is relatively efficient to produce an accurate representation of the tissue mechanical modeling, the required time to compute the model outputs is a constrain for when the decision time is limited. This challenge is highlighted in certain applications such as surgical procedures [8].

Considering mathematical complexity of continuum approach and computational costs of structural approach, artificial intelligence (AI)-based approach as an alternative advantageous methodology could be utilized to predict the tissue response based on the historical datasets, which potentially increase the modeling accuracy and minimizes the computation time for real-time applications [17]. Accordingly, artificial neural networks (ANNs) are a family of statistical learning algorithms, which have been used by many researchers to predict the mechanical behavior of materials under diverse conditions such as monotonic and cyclic loadings [18, 19]. In other words, ANNs offer an effective alternative for constitutive models in order to predict the complex mechanical responses. Hence, several ANN architectures have been used so far. Multilayer back-propagation neural network learning algorithms have been proven to be an effective and accurate tool, especially when there is sufficient training data. The capacity of the algorithm has been examined here for the prediction of the mechanical behavior of human ureter. To manage ill-posed problems caused by the non-physical nature of machine learning, physics-informed neural networks were applied to predict tissue dynamics in the constrained parameter spaces [20].

Therefore, the main objectives of this study are to i) obtain the constitutive model parameters of the ureteral sample tissues by utilizing the biaxial loading strategy and solving the pertinent inverse problem, ii) predict the nonlinear tissue response by training ANN with the same experimental data, and iii) evaluate the potential of ANN for modeling the mechanical behavior of soft biological tissues.

2. Materials and Methods

Among several experimental setups, the biaxial tensile test is suitable to investigate the anisotropic response of the opened-up (stress-free) ureteral walls [5, 21]. Consequently, in order to investigate the mechanical behavior of human ureter tissue, biaxial tensile test paradigm was designed and implemented. Next, to obtain the unknown parameters of nonlinear constitutive models, in conjunction with the biaxial test setup, the genetic optimization algorithm (GA) was employed in the mentioned inverse problem. To evaluate the capability of neural networks for following the mechanical behavior of the ureter tissue, multi-layer perceptron (MLP) network was designed and trained using obtained experimental data. The overall workflow of this study is shown in Figure 1. A paper that reports technically original research output, which has academic and/or industrial contributions. Original papers undergo full peer review.

2.1 Analytical Models

In order to incorporate the tissue response into the framework of constitutive modeling, the ureter was modeled as a hyperelastic material and then, two strain energy density (SED) functions were employed to characterize the stored energy in the ureteral wall as a result of the applied deformation; Fung hyperelastic and the combined Holzapfel-Delfino (H-D) SED function [12, 22-24].

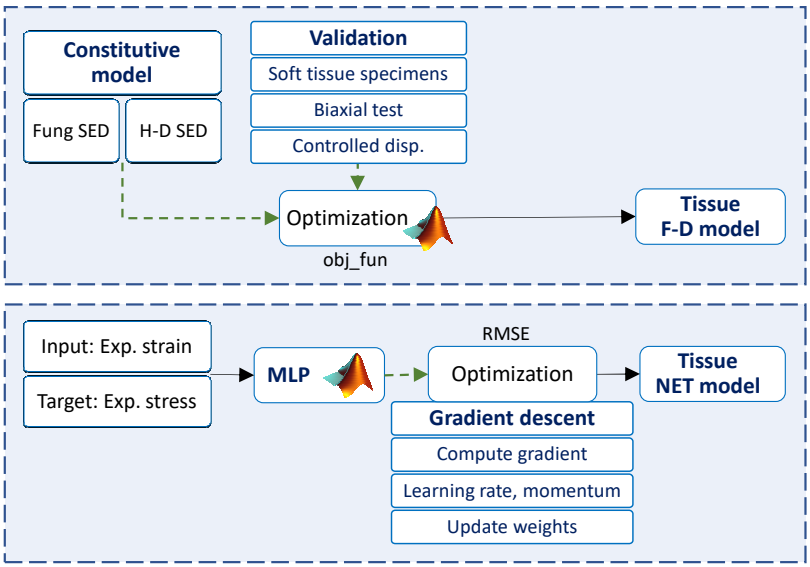

Fig. 1. Overall view of the study.

By derivation of SED function, W, with respect to the right Cauchy-Green deformation tensor, C, the stress tensor can be computed as follows:

$$\sigma = 2J^{-1}FW_C F^T, \qquad C = F^T F \tag{1}$$

in which σ is the Cauchy stress tensor, F is the deformation gradient tensor, J is the volume change ratio (=det F), and $W_C=\partial W/\partial C$. Furthermore, the stress can be calculated in the deformed direction of fibers, a, as:

$$\sigma_a = J^{-1}\lambda_a W_a, \qquad \lambda_a{}^2 = A : C \tag{2}$$

where λ is the stretch along the preferred direction a_0, $A=a_0\otimes a_0$ is the structural tensor, and $W_a=\partial W/\partial\lambda_a$ [25]. Notably, the assumption of incompressibility ($J=\lambda_1\lambda_2\lambda_3=1$) was considered for the tissue based on the weak compressibility of its fluid and solid contributions:

$$\lambda_3 = \lambda_1{}^{-1}\lambda_2{}^{-1}, \qquad \sigma_a = -p + \lambda_a W \tag{3}$$

for which the scalar p can be identified as a hydrostatic pressure.

The first applied model in this study was a two-dimensional form of Fung-type model that describes the nonlinear behavior of the tissue with an exponential function:

$$W(Q) = \frac{1}{2}c(e^Q - 1), \; Q(E) = a_1 E_{11}{}^2 + a_2 E_{22}{}^2 + 2a_3 E_{11}E_{22} \tag{4}$$

in which $E=(C-I)/2$ is the Green-Lagrange strain tensor, where I is the identity tensor, and c, a_1, a_2, and a_3 are four constitutive parameters. These parameters cannot be chosen arbitrarily but, should satisfy the stress-free reference condition. In particular, if $c > 0$, then (4) is locally convex if and only if $a_1 > 0$, $a_2 > 0$ and $a_1a_2 > a_3{}^2$ [12]. The biaxial Cauchy stress components in the two directions for the incompressible Fung model were then calculated as [26]:

$$Q(\lambda_1,\lambda_2) = \frac{1}{4}(a_1(\lambda_1^2-1)^2 + a_2(\lambda_2^2-1)^2 + 2a_3(\lambda_1^2-1)(\lambda_2^2-1)) \tag{5}$$

$$\sigma_1^F = \frac{1}{2}c\lambda_1^2[a_1(\lambda_1^2-1) + a_3(\lambda_2^2-1)]\times\exp[Q(\lambda_1,\lambda_2)] \tag{6}$$

$$\sigma_2^F = \frac{1}{2}c\lambda_2^2[a_2(\lambda_2^2-1) + a_3(\lambda_1^2-1)]\times\exp[Q(\lambda_1,\lambda_2)] \tag{7}$$

The second employed model was the H-D SED function that represents the anisotropic behavior of the tissues in terms of invariants of deformation tensor:

$$W = c_1(I_1-3) + D_1[\exp(D_2(I_1-3)) - 1] + \frac{k_1}{2k_2}[\exp(k_2(I_4-1)^2) - 1] \tag{8}$$

where I_1 and I_4 are the first and forth invariants of C ($I_1 = \mathrm{tr}C$; $I_4 = A : C = \lambda_a{}^2$), a is the circumferential direction (axis '1'), and c_1, D_1, D_2, k_1, and k_2 are the model parameters. The terms (I_1-3) and (I_4-1) satisfy the stress-free reference condition. Therefore, the Cauchy stresses in the two axes (σ_3=0: $p=\lambda_3 W_3$) are as follow [26]:

$$\sigma_1{}^{H-D} = 2(\lambda_1{}^2 - \lambda_1{}^{-2}\lambda_2{}^{-2})[c_1 + D_1D_2\exp(D_2(\lambda_1^2+\lambda_2^2+\lambda_1{}^{-2}\lambda_2{}^{-2}-3))] + 2k_1\lambda_1{}^2(\lambda_1{}^2-1)[\exp(k_2(\lambda_1{}^2-1)^2)] \tag{9}$$

$$\sigma_2{}^{H-D} = 2(\lambda_2{}^2 - \lambda_1{}^{-2}\lambda_2{}^{-2})[c_1 + D_1D_2\exp(D_2(\lambda_1^2+\lambda_2^2+\lambda_1{}^{-2}\lambda_2{}^{-2}-3))] \tag{10}$$

Experimental data then were fitted to the Cauchy stress of each model using GA optimization implemented in Matlab (The Mathworks, Inc., Natick, MA) and the parameters of the constitutive models were obtained for each data set. As such, the following objective function was defined to be minimized in the optimization problem:

$$Er = \sqrt{\frac{\sum\left(\sigma_{anl}(i) - \sigma_{exp}(i)\right)^2}{\sum\sigma_{exp}(i)^2}} \tag{11}$$

where Er is the misfit measure and $\sigma_{exp}(i)$ and $\sigma_{anl}(i)$ represent the experimental and analytical stress at the time i, respectively. In order to enhance the efficiency of the optimization procedure, the lower (was set to be zero) and upper bounds for the unknown parameters were defined. The obtained parameters were checked to be consistent with the introduced convexity requirements for the Fung model.

2.2 Artificial Neural Network Model

The term 'artificial neural networks (ANN)' stands for the software or hardware simulators concerning semi-parallel data processing. These simulators are compounded of many mutually connected neurons and mimic the function of biological brain structure [27]. In the present effort, in order to predict the soft tissue response to a mechanical excitation as an alternative for constitutive models, a feedforward MLP neural network was used. The MLP architecture, which has maximum practical importance, consisted of a set of input and hidden layers, and one output layer, in which, input data propagates through the network, layer by layer. The architecture of the MLP network with one hidden layer is represented in Figure 2. As illustrated in the figure, for a set of training samples {(a(k), t(k))}, where $a^{(i)} \in R^n$ and $t^{(i)} \in R^m$ are the input and output vectors in n- and m-dimensional space, N_k inputs are fed into the first layer of N_h hidden layers. $w_{ij}{}^{(l)}$ is a weighting coefficient on the connection between the ith neuron in layer (l-1) to jth neuron in layer l. The goal of the training process is the finding of optimum weights for

the trained network with historical datasets of the biaxial test data (input: strain; target: stress) to minimize the error function between the ANN output, z_i, and target vectors t_i. Hence, the root mean squared error (RMSE) function that is the most frequently used criteria in the literature to evaluate the performance of ANN models, can be defined for sample p at the output layer as:

$$E^{(p)} = \frac{1}{2}\sum_{i=1}^{m}(t_i^{(p)} - z_i^{(p)})^2 \tag{12}$$

Notice that the optimum weights will be achieved through minimizing the summed or overall squared error function $E = \sum_1^p E^{(p)}$.

2.2.1 Learning Strategy

For training the MLP model based on the back-propagation algorithm, the focus is on the gradient descent-based delta method for nonlinear least-squares optimization [28, 29]. The generalized form of delta rule was used for the learning procedure of the network. According to the delta rule for single-layer networks, weights are modified towards minimizing RMSE in each step of learning as below [30]:

$$w^{(k)} - w^{(k-1)} = -\eta\frac{\partial E}{\partial w} = -\eta f'(y) \tag{13}$$

or, for each element of the weighting matrix:

$$\Delta w_{ij} = w_{ij}^{k} - w_{ij}^{(k-1)} = \eta(t_j - y_j)f'(y) \tag{14}$$

where η is a learning rate constant, f is an activation function of neurons, y denotes the output of layer before passing through the activation function, and $w^{(k)}$ and $w^{(k-1)}$ are weight matrices in (k)th and (k-1)th iterations, respectively. Generalizing the learning rule for a single layer network in which the weighting coefficient matrix is obtained by minimizing the error between the output and target vectors, the loss function can be computed using backward gradient flow that is known as the "feedforward back-propagation" approach. Mathematical formulation and computational procedures of this scenario have been presented in Appendix 1.

For speeding the convergence and avoiding local minima in the back-propagation algorithm, using an additional term called momentum can be helpful. The idea behind using momentum is to stabilize the weight change by making nonradical revisions using a combination of the gradient decreasing term with a fraction of the weight change [31]:

$$\Delta w^{(k)} = -\eta\frac{\partial E^{(p)}}{\partial w} + \alpha\Delta w^{(k-1)} \tag{15}$$

where gives the system a certain amount of inertia as an attempt to escape the local minima or saddle points by stepping in the direction of the velocity vector, α ($0 < \alpha < 0.9$), rather than the raw gradient.

2.3 Biaxial In-Vitro Tensile Test on the Human Ureter Specimens

Since the preparation of the samples and the experimental setup is described in the previous paper ([5]), only the summary of the main aspects is presented here.

2.3.1 Sample Preparation

The healthy ureter samples were extracted from human and cleaned off during the preparation and then, stored in physiological 0.9% saline before testing. Measurements were completed within 10 hours after the extraction. The specimens were cut along the longitudinal axis and shaped into squares with 6 mm sides in order to suit our biaxial test setup. The specimen thicknesses were measured using a micrometer and the average thickness was used in the formulations.

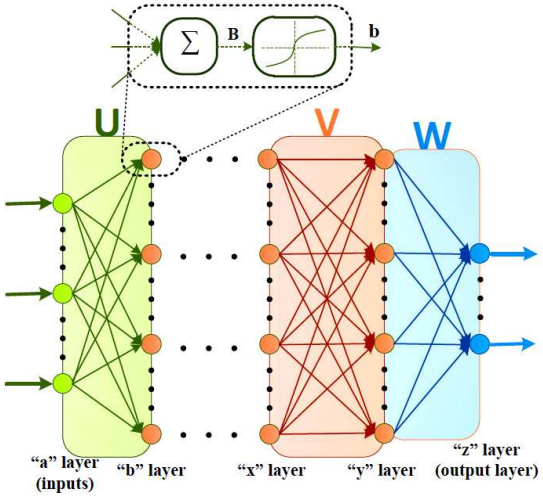

Fig. 2. Configuration of the MLP neural network model.

2.3.2 Experimental Setup and Testing Procedure

A planar biaxial test device, with strain measurement capability, was utilized to obtain the stress/strain correlation along the circumferential and longitudinal axes of the specimens (Figure 3). The clamps of the system were able to directly hold samples with dimensions more than 5*5mm^2 without damaging the tissue. After fixing the specimens into the device, they were preloaded with 0.01N loading along both axes to avoid offset of exerted forces on the ends. The loadings were applied with the rate of 0.02mm/s through four micro stepper motors in both directions and the tensile forces were measured by two UMAA 2 kilogram-force load cells (Dacell Co., Ltd, Korea Corporation, Korea). For the purpose of deformation measurement, an USB digital microscope camera was used and the output data was processed with the ImageJ package to obtain stretch in each direction. The stress-strain curve for each specimen was obtained in the two axes ((1) and (2) are corresponded to the circumferential and longitudinal directions, respectively) for which the experimental stresses were computed as follows:

$$\sigma_1^{\exp} = \lambda_1 \frac{F_1}{l_2 t} \tag{16}$$

$$\sigma_2^{\exp} = \lambda_2 \frac{F_2}{l_1 t} \tag{17}$$

where λ_1 and λ_2 are the stretch ratios, F_1 and F_2 are the measured forces by the load cells, t is the thickness of the samples, and l_1 and l_2 are the unloaded widths of the samples in the two directions.

3. Results

Because of the anisotropic and nonlinear nature of the ureter wall, two nonlinear constitutive models were used for modeling the mechanical behavior of the tissue. In the experiment phase, since some specimens were unsuitable for mechanical testing (were degenerated during the preparation), the resultant stress-strain data of three samples in the axial and circumferential directions were employed in the optimization algorithms to obtain the constitutive parameters. Table 1 represents the Fung and H-D best-fit material parameters for all the existing data. In the next phase of the study, the MLP neural network was developed in order to establish the relationship between circumferential and longitudinal stresses (target) and strains (input). For this purpose, Matlab software was used for creating, training, validating, and testing the network. The optimal number of 8 neurons in one hidden layer with the learning rate, η = 0.4, and momentum, α = 0.8, was selected for modeling the tissue behavior. Figure 4 displays the experimental versus the optimized results of ANN and constitutive models revealing that both approaches are capable to model the tissue responses in two directions.

In order to further investigate the potential of neural networks, other types of networks were subjected to the training process. In particular, the recurrent neural network (RNN) as well as long short-term memory RNN (LSTM) were well-able to characterize the tissue nonlinear behavior in our datasets and specifically, an RNN model with 7 neurons and 3 delays and the same learning rate and momentum had the best-fit result. There were no significant differences between the performance of feedforward and recurrent neural network in the RMSE values.

Fig. 3. Different parts of the biaxial test device; clamps for direct holding of the tissue, digital camera, and data synchronization.

Table 1. The obtained human ureter parameters of the two hyperelastic constitutive models.

Fung Model*

Parameters	c (MPa)	a_1	a_2	a_3
Ureter 1	1.9457	0.1089	0.1435	0.0394
Ureter 2	0.1122	0.9281	0.5951	0.4997
Ureter 3	0.3262	0.3556	0.9223	0.1229

H-D Model

Parameters	c_1 (MPa)	D_1 (MPa)	D_2	k_1 (MPa)	k_2
Ureter 1	0.0016	0.2038	0.3798	-0.0068**	0.1239
Ureter 2	0.0009	0.0097	1.2748	0.0145	0.6312
Ureter 3	0.0000	0.0802	0.8786	-0.1592**	0.3665

* The convexity requirements were satisfied for the Fung model.

** The negative number for k_1 was allowed to adjust the model into both directions.

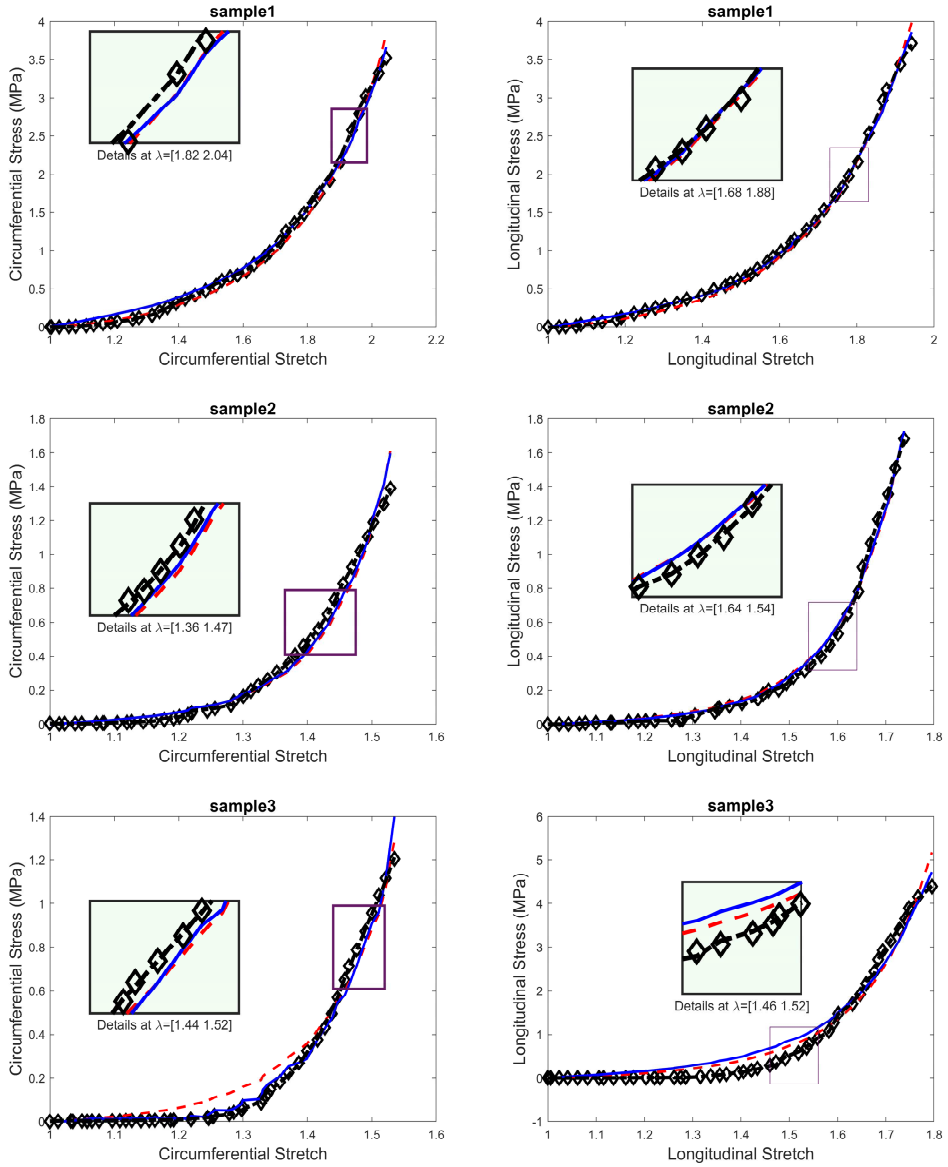

Fig. 4. Comparison between the experimental and optimized forces for each sample (◊: Experiment, —: H-D model, - - -: Fung model, and - . - . -: ANN model).

3.1 Statistical Analysis

The statistical comparison between nonlinear constitutive models and ANN performances are presented in Table 2 and depicted in Figures 5 and 6. Accordingly, the ANN model has lower amounts of RMSE and mean absolute percentage error (MAPE) for predicting the nonlinear response of human ureter in both directions (Figure 5). As shown in Figure 6, the ANN predictions are even better especially under low strains at which the exact characterization of tissue nonlinearity adds further computational cost to the developed constitutive models.

4. Discussion

This paper presented two different approaches to modeling the ureter tissue response against external loading. An analytical approach was the inverse parameter identification of the nonlinear constitutive equations and the alternative method was considering AI-based modeling without mechanical elements. The experimental data derived from the biaxial tension test on the human ureter was used for obtaining the constitutive parameters and training the MLP network.

Table 2. The statistical comparison between two mechanical constitutive models and ANN.

Model type	Direction	RMSE	MAPE
Fung	Circumferential	0.0658	0.9789
H-D		0.0538	0.7632
ANN		0.0116	0.0287
Fung	Longitudinal	0.1077	1.5710
H-D		0.1055	2.6220
ANN		0.0148	0.0399

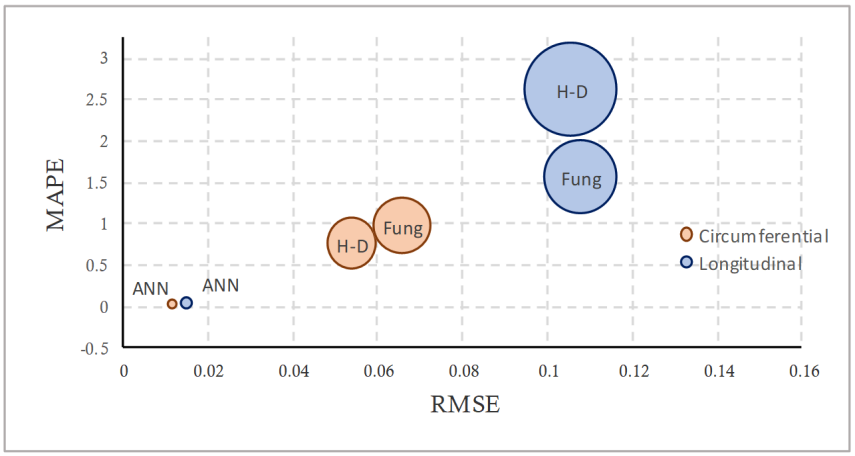

Fig. 5. The statistical comparison between models based on the averaged RMSE and MAPE (Table 2).

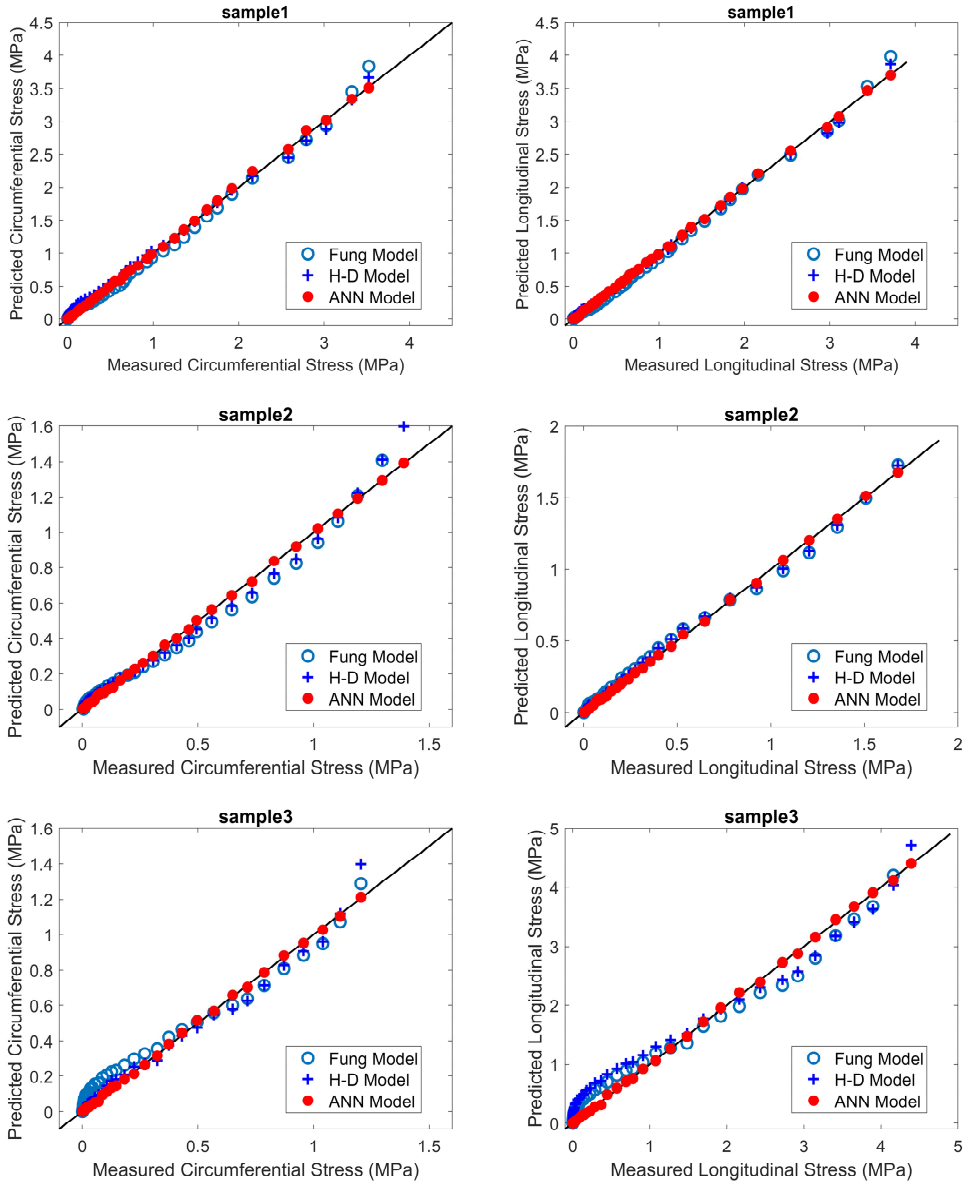

Fig. 6. The predicted values of the MLP and constitutive mechanical models versus the measured values of stress for human ureter samples.

In the framework of constitutive modeling, the efficiency of a model is directly dependent on the capability of the selected function for providing accurate reflections of the tissue morphology. In other words, each term of a constitutive model should have a physical interpretation from the biomechanical point of view. Obviously, characterizing the more complicated behavior adds further terms to mechanical equations (e.g. exponential functions) and therefore, adds the computational cost. Moreover, to

ensure mechanical and mathematical reliability, such constitutive models should remain consistent with the convexity requirements. Nevertheless, the interpretable, modifiable, and upgradable nature of such models is of benefit to provide an explicit mechanical description especially when time is not concerned. Thus, the overall response of ureter was acceptably described with both hyperelastic models. Although there were no significant differences in the performance of the two models, the Fung model had a slightly better fit to the datasets.

Based on the obtained results, on average the higher stiffness of the ureter tissues in the axial direction is detectable ($a_2>a_1$ in the Fung model and $k_1<0$ in the H-D model). This observation indicates that the collagen fiber organization is more effective in this direction. In fact, the tissue response in such tissues is mostly dependent on two structural components making the mechanical sense: collagen (strength) and elastin (nonlinearity). In the lower strains (and strain rates), each of these elements has a contribution in the tissue response while, in the higher strains, the collagen networks play the dominant role in providing the mechanical strength of the tissue. As shown in Figure 6, in the lower strains, both SED functions are potentially error-prone due to the high level of nonlinearity, specifically in the longitudinal direction.

To address the mentioned challenges in the constitutive modeling approach, the advantages of AI-based techniques in real-time applications are significant. In fact, instead of developing a structural model, the tissue is simplified as a programmed controller by which each in-range input would have a pre-trained output. Thus, a trained ANN with experimental data (or even with analytical or computational data) can practically be used in real-time applications that are broadly discussed in recent years. According to the presented results, the ANN models not only can follow up the tissue response during the entire loading phase but also can accurately mimic the tissue nonlinearity in the low and high strain amplitudes.

5. Conclusion

In conclusion, both explored approaches in this study were practically able to predict the nonlinear behavior of ureter tissue under biaxial tensile test. The hyperelastic functions can be used in the FE and FSI analyses where the comparative results of healthy and diseased states are of importance. In comparison, physics-informed ANN modeling is an alternative mathematical potential that can realize the complexity of living tissue behavior. As such, defining material properties based on the mathematical potential of ANN models within the FE software would provide a more reliable biomechanical framework for a true reflection of the complexity of living tissues. In other words, since biological materials (unlike classical engineering materials) interact with their environment, the need for such a framework sounds crucial to reconsider equations of classical physics (the conservation laws of mass, momentum, and energy, laws of thermodynamics) and instead, train the constitutive model based on MLP or RNN models. To evaluate, the ANN modeling can be extended to incorporate time and rate dependent behavior of biological and biomedical materials. More investigations are required to specify the advantages and drawbacks of types of neural networks for such an application. Moreover, developing a control system based on the integration of these two approaches for real-time robotically-assisted surgery would be another perspective for future work. In the end, the potential of AI seems to be far more in the context of eHealth applications that its domain is growing rapidly.

Appendix A

In the MLP model, we assume that the linear and sigmoid activation functions are differentiable functions of the total input, given by:

$$z_k = F^{(z)}(Z_k) \qquad where:\ Z_k = \sum_j w_{jk}\bar{Y} + \theta^{(z)}_k \tag{A.1}$$

where θ is the bias value. Similar to the delta rule for single layer networks, the learning procedure can be generalized by modifying the weights proportional to the gradient descent of the error function for every training sample p as below:

$$w^{(k)}_{jk} - w^{(k-1)}_{jk} = -\eta\frac{\partial E^{(p)}}{\partial w_{jk}} \tag{A.2}$$

using the chain rule, we can write:

$$\frac{\partial E^{(p)}}{\partial w_{jk}} = \frac{\partial E^{(p)}}{\partial Z^p_k}\frac{\partial Z^p_k}{\partial w_{jk}} \tag{A.3}$$

By calculating the second factor from (A.1) $\partial Z^p_k/\partial w_{jk} = y^p_j$ and defining the error signal for output layer z as $\delta^{p-z}_k = -\partial E^{(p)}/\partial Z^p_k$, the equation A.2 can be written as follow:

$$[w^{(k)}_{jk} - w^{(k-1)}_{jk}]^{(p)} = \eta\delta^{p-z}_k y^p_j \tag{A.4}$$

again, δ^{p-z}_k can be computed using the chain rule in the form of:

$$\delta^{p-z}_k = -\frac{\partial E^{(p)}}{\partial Z^p_k} = -\frac{\partial E^{(p)}}{\partial z^p_k}\frac{\partial z^p_k}{\partial Z^p_k} \tag{A.5}$$

The second fraction in (A.5) is the derivative of the activation function $F^{(z)}$ in the equation A.1 for kth neuron as $\partial z^p_k/\partial Z^p_k = F'(Z^p_k)$. To compute the first factor of (A.5), the equation (13) is employed and thus we have $\partial E^{(p)}/\partial z^p_k = -(t^{(p)} - z^{(p)})$. Substituting in the equation A.5 yields:

$$\delta^{p-z}_k = (t^p_k - z^p_k)F'(Z^p_k) \tag{A.6}$$

All the computations for error signal δ are for z layer which assumed to be an output layer as shown in figure 2. Again, using the chain rule, the error signals for hidden layers can be computed recursively and by propagating the signals backward through the network and computing local and upstream gradients, the updated weights would be obtained.

Author Contributions

The manuscript was written through the contribution of all authors. This contribution included planning the modeling scheme, conducting the experiments, and developing and validating the mathematical and analytical models. All authors discussed the results, reviewed and approved the final version of the manuscript.

Acknowledgments

Not applicable.

Conflict of Interest

The authors declared no potential conflicts of interest with respect to the research, authorship and publication of this article.

Funding

The authors received no financial support for the research, authorship and publication of this article.

Data Availability Statements

The datasets generated and/or analyzed during the current study are available from the corresponding author on reasonable request.

Nomenclature

σ	Cauchy stress tensor	$E^{(p)}$	Mean squared error function
W	Strain energy density function	z_i	ANN output vector
F	Deformation gradient tensor	t_i	Target vector
C	Cauchy-Green deformation tensor	y_i	Output of hidden layer
J	Volume change ratio	w	Weight matrix
λ_a	Stretch along the preferred direction a_0	f	Activation function
A	Structural tensor	η	Learning rate constant
E	Green-Lagrange strain tensor	α	Momentum constant
p	Indeterminate multiplier serves as a hydrostatic pressure	$F_{1,2}$	Measured forces by the load cells
I_1	First invariant of C	t	Thickness of the samples
I_4	Forth invariant of C	$l_{1,2}$	Widths of the samples in the two directions
Er	Error function		

References

[1] Autorino, R., H. Zargar, and J.H. Kaouk, Robotic-Assisted Laparoscopic Surgery: Recent Advances in Urology, *Fertility and Sterility*, 102(4), 2014, 939-949.
[2] Vahidi, B., et al., A Mathematical Simulation of the Ureter: Effects of the Model Parameters on Ureteral Pressure/Flow Relations, *Journal of Biomechanical Engineering*, 133(3), 2011, 031004.
[3] Keating, M.A., et al., Changing Concepts in Management of Primary Obstructive Megaureter, *The Journal of Urology*, 142(2), 1989, 636-640.
[4] Shokeir, A. and R. Nijman, Primary Megaureter: Current Trends in Diagnosis and Treatment, *BJU International*, 86(7), 2000, 861-868.
[5] Rassoli, A., et al., Biaxial Mechanical Properties of Human Ureter under Tension, *Urology Journal*, 11(3), 2014, 1678-1686.
[6] Picinbono, G., et al., Improving Realism of a Surgery Simulator: Linear Anisotropic Elasticity, Complex Interactions and Force Extrapolation, *The Journal of Visualization and Computer Animation*, 13(3), 2002, 147-167.
[7] Greenleaf, J.F., M. Fatemi, and M. Insana, Selected Methods for Imaging Elastic Properties of Biological Tissues, *Annual Review of Biomedical Engineering*, 5(1), 2003, 57-78.
[8] Moreira, P., et al., Viscoelastic Model Based Force Control for Soft Tissue Interaction and Its Application in Physiological Motion Compensation, *Computer Methods and Programs in Biomedicine*, 116(2), 2014, 52-67.
[9] Hostettler, A., et al., Bulk Modulus and Volume Variation Measurement of the Liver and the Kidneys in Vivo Using Abdominal Kinetics During Free Breathing, *Computer Methods and Programs in Biomedicine*, 100(2), 2010, 149-157.
[10] Barnes, S., et al., Frequency Dependent Viscoelastic Properties of Porcine Bladder, *Journal of the Mechanical Behavior of Biomedical Materials*, 42, 2015, 168-176.
[11] Mow, V.C. and R. Huiskes, *Basic Orthopaedic Biomechanics & Mechano-Biology*, Lippincott Williams & Wilkins, 2005.
[12] Holzapfel, G.A., T.C. Gasser, and R.W. Ogden, A New Constitutive Framework for Arterial Wall Mechanics and a Comparative Study of Material Models, *Journal of Elasticity and the Physical Science of Solids*, 61(1-3), 2000, 1-48.
[13] Mihai, L.A., et al., A Comparison of Hyperelastic Constitutive Models Applicable to Brain and Fat Tissues, *Journal of the Royal Society Interface*, 12(110), 2015, 20150486.
[14] Snedeker, J.G., et al., Strain-Rate Dependent Material Properties of the Porcine and Human Kidney Capsule, *Journal of Biomechanics*, 38(5), 2005, 1011-1021.
[15] Sokolis, D.P., Multiaxial Mechanical Behaviour of the Passive Ureteral Wall: Experimental Study and Mathematical Characterisation, *Computer Methods in Biomechanics and Biomedical Engineering*, 15(11), 2012, 1145-1156.
[16] Stylianopoulos, T. and V.H. Barocas, Volume-Averaging Theory for the Study of the Mechanics of Collagen Networks, *Computer Methods in Applied Mechanics and Engineering*, 196(31-32), 2007, 2981-2990.
[17] Hashemi, M.S., et al., A Novel Machine Learning Based Computational Framework for Homogenization of Heterogeneous Soft Materials: Application to Liver Tissue, *Biomechanics and Modeling in Mechanobiology*, 2019, 1-12.
[18] El Kadi, H., Modeling the Mechanical Behavior of Fiber-Reinforced Polymeric Composite Materials Using Artificial Neural Networks—a Review, *Composite Structures*, 73(1), 2006, 1-23.
[19] Schöllhorn, W., Applications of Artificial Neural Nets in Clinical Biomechanics, *Clinical Biomechanics*, 19(9), 2004, 876-898.
[20] Alber, M., et al., Integrating Machine Learning and Multiscale Modeling—Perspectives, Challenges, and Opportunities in the Biological, Biomedical, and Behavioral Sciences, *NPJ Digital Medicine*, 2(1), 2019, 1-11.
[21] Kural, M.H., et al., Planar Biaxial Characterization of Diseased Human Coronary and Carotid Arteries for Computational Modeling, *Journal of Biomechanics*, 45(5), 2012, 790-798.
[22] Fung, Y., K. Fronek, and P. Patitucci, Pseudoelasticity of Arteries and the Choice of Its Mathematical Expression, *American Journal of Physiology-*

Heart and Circulatory Physiology, 237(5), 1979, H620-H631.
[23] Delfino, A., et al., Residual Strain Effects on the Stress Field in a Thick Wall Finite Element Model of the Human Carotid Bifurcation, *Journal of Biomechanics*, 30(8), 1997, 777-786.
[24] Tang, D., et al., 3d Mri-Based Anisotropic Fsi Models with Cyclic Bending for Human Coronary Atherosclerotic Plaque Mechanical Analysis, *Journal of Biomechanical Engineering*, 131(6), 2009.
[25] Weiss, J.A., B.N. Maker, and S. Govindjee, Finite Element Implementation of Incompressible, Transversely Isotropic Hyperelasticity, *Computer Methods in Applied Mechanics and Engineering*, 135(1-2), 1996, 107-128.
[26] Holzapfel, G.A. and R.W. Ogden, On Planar Biaxial Tests for Anisotropic Nonlinearly Elastic Solids. A Continuum Mechanical Framework, *Mathematics and Mechanics of Solids*, 14(5), 2009, 474-489.
[27] Müller, B., J. Reinhardt, and M.T. Strickland, *Neural Networks: An Introduction*, Springer Science & Business Media, 2012.
[28] Nocedal, J. and S. Wright, *Numerical Optimization*, Springer Science & Business Media, 2006.
[29] Sadati, S.H., J.A. Kaklar, and R. Ghajar, Application of Artificial Neural Networks in the Estimation of Mechanical Properties of Materials, Artificial *Neural Networks - Industrial and Control Engineering Applications*, Croatia, 2011.
[30] Kröse, B., et al., An Introduction to Neural Networks, *Journal of Computer Science*, 48, 1993.
[31] Bishop, C.M., *Neural Networks for Pattern Recognition*, Oxford University Press, 1995.

ORCID iD

Behzad Seyfi https://orcid.org/0000-0002-5503-4203
Aisa Rassoli https://orcid.org/0000-0002-4612-2607
Milad Imeni Markhali https://orcid.org/0000-0003-0244-3107
Nasser Fatouraee https://orcid.org/0000-0002-5714-027X

How to cite this article: Seyfi B., Rassoli A., Imeni M., Fatouraee N. Characterization of the Nonlinear Biaxial Mechanical Behavior of Human Ureter using Constitutive Modeling and Artificial Neural Networks, *J. Appl. Comput. Mech.*, 8(4), 2022, 1186–1195. https://doi.org/10.22055/JACM.2020.33703.2272